AFRL-RV-PS-
TR-2020-0115

AFRL-RV-PS-
TR-2020-0115

BAYESIAN DIFFERENTIAL MOMENT TENSOR INVERSION OF CLUSTERED NUCLEAR TESTS

Zhongwen Zhan, et al.

California Institute of Technology
1200 East California Blvd., MC 252-21
Pasadena, CA 91125

30 December 2020

Final Report

AIR FORCE RESEARCH LABORATORY
Space Vehicles Directorate
3550 Aberdeen Ave SE
AIR FORCE MATERIEL COMMAND
KIRTLAND AIR FORCE BASE, NM 87117-5776

DTIC COPY

NOTICE AND SIGNATURE PAGE

AFRL-RV-PS-TR-2020-0115 HAS BEEN REVIEWED AND IS APPROVED FOR PUBLICATION IN ACCORDANCE WITH ASSIGNED DISTRIBUTION STATEMENT.

//SIGNED//	//SIGNED//
_____	_____
Dr. Raymond J. Willemann	Erin N. Pettyjohn, Chief
Program Manager/AFRL/RVB	AFRL Geospace Technologies Division

REPORT DOCUMENTATION PAGE

Form Approved
OMB No. 0704-0188

1. REPORT DATE *(DD-MM-YYYY)*	**2. REPORT TYPE**	**3. DATES COVERED** *(From - To)*
20-12-2020	Final Report	27 Sep 2018 – 28 Sep 2020

4. TITLE AND SUBTITLE
Bayesian Differential Moment Tensor Inversion of Clustered Nuclear Tests

5a. CONTRACT NUMBER
FA9453-18-C-0058

5b. GRANT NUMBER

5c. PROGRAM ELEMENT NUMBER
62601F

6. AUTHOR(S)
Zhongwen Zhan, Zhe Jia, and Donald V. Helmberger

5d. PROJECT NUMBER
1010

5e. TASK NUMBER
EF133207

5f. WORK UNIT NUMBER
V1HN

7. PERFORMING ORGANIZATION NAME(S) AND ADDRESS(ES)
California Institute of Technology
1200 East California Blvd., MC 252-21
Pasadena, CA 91125

8. PERFORMING ORGANIZATION REPORT NUMBER

9. SPONSORING / MONITORING AGENCY NAME(S) AND ADDRESS(ES)
Air Force Research Laboratory
Space Vehicles Directorate
3550 Aberdeen Avenue SE
Kirtland AFB, NM 87117-5776

10. SPONSOR/MONITOR'S ACRONYM(S)
AFRL/RVBN

11. SPONSOR/MONITOR'S REPORT NUMBER(S)
AFRL-RV-PS-TR-2020-0115

12. DISTRIBUTION / AVAILABILITY STATEMENT
Approved for public release; distribution is unlimited (AFMC-2020-0591 dtd 22 Dec 20).

13. SUPPLEMENTARY NOTES

14. ABSTRACT
Accurate seismic moment tensor measurement plays an important role in nuclear test monitoring and yield estimation. However, conventional source moment tensor inversions require accurate Green's functions between source and receivers, and rely mostly on regional data coverage which could be sparse or incomplete in azimuthal coverage. In this study, we propose a new method, differential moment tensor inversion (diffMT), which adopts relative measurements to remove the path effects shared by different events at the same station, thereby improving the accuracy of source parameter determination. We apply diffMT to the four nuclear tests conducted by North Korea from 2009 to 2016. We found that, compared with the traditional method of waveform-based moment tensor inversion, diffMT more tightly constrains the moment tensor components of these nuclear tests, measures the energy release of these events more accurately, and better distinguishes their isotropic and tectonic release components. Our results provide potential insights on the explosion mechanisms and physical processes of North Korea's nuclear tests.

15. SUBJECT TERMS
Moment tensor inversion, surface waves, body waves

16. SECURITY CLASSIFICATION OF:			**17. LIMITATION OF ABSTRACT**	**18. NUMBER OF PAGES**	**19a. NAME OF RESPONSIBLE PERSON**
a. REPORT	**b. ABSTRACT**	**c. THIS PAGE**			Dr. Raymond J. Willemann
Unclassified	Unclassified	Unclassified	Unlimited	30	**19b. TELEPHONE NUMBER** *(include area code)*

This page is intentionally left blank.

Table of Contents

Figures

Tables

1. SUMMARY

Accurate seismic moment tensor measurement plays an important role in nuclear test monitoring and yield estimation. However, conventional source moment tensor inversions require accurate Green's functions between source and receivers, and rely mostly on regional data coverage which could be sparse or incomplete in azimuthal coverage. In this study, we propose a new method, differential moment tensor inversion (diffMT), which adopts relative measurements to remove the path effects shared by different events at the same station, thereby improving the accuracy of source parameter determination. We apply diffMT to the four nuclear tests conducted by North Korea from 2009 to 2016. We found that, compared with the traditional method of waveform-based moment tensor inversion, diffMT more tightly constrains the moment tensor components of these nuclear tests, measures the energy release of these events more accurately, and better distinguishes their isotropic and tectonic release components. Our results provide potential insights on the explosion mechanisms and physical processes of North Korea's nuclear tests.

2. INTRODUCTION

The moment tensor is a 3*3 tensor, which provides a point-source approximation of the radiation pattern and energy release of a seismic event. Moment tensors can be decomposed to isotropic, double couple (DC), and compensated linear vector dipole (CLVD) components. Different combinations of these components typically manifest well the first order physics of different types of seismic events, such as natural earthquakes, collapses, and nuclear explosions. Therefore, in the monitoring and discrimination of nuclear tests, the moment tensor inversion of seismic data is very important [Alvizuri and Tape, 2018; Cesca et al., 2017; Ford et al., 2009]. In the past few decades, moment tensor inversion has gradually progressed from ray and polarity-based seismic processing to waveform-based inversion [Ekström et al., 2012; Kanamori and Rivera, 2008; Zhu and Helmberger, 1996]. At the theoretical level, Tape and Tape [2012; 2013; 2015] proposed a mathematically elegant and intuitive way to view the moment tensor solution and test the explosion hypothesis. Zhu and Ben-Zion [2013] developed a new parameterization of moment tensors with well-defined finite ranges for non-linear waveform-based source inversion. All of these applications and theoretical progress, together with continuously improving Earth models and computational methods, promise great potential for using moment tensors in nuclear monitoring. This progress in moment tensor theory and source inversion applications, as well as the continuously improving Earth structural models and computational methods, reveals great potential for moment tensor inversion for the nuclear test monitoring.

Despite its great successes in event discrimination and yield estimation, full moment tensor inversion for shallow sources still face major challenges. Since the moment tensor inversion requires knowledge of the earth structure between the source and receivers, robust moment tensor solutions are usually only retrievable at long periods (e.g. T>10s, [Ford et al., 2009]) that are insensitive to small-scale structural heterogeneities. However,

different from tectonic earthquakes, explosions usually have a limited energy release and spatial extent, with limited near-field coverage. Their seismic signals at long periods and large distances can be difficult to observe, posing data deficiency problems for long period moment tensor inversions. For the shorter period seismic waveforms, the propagation through complex paths with rough topography and 3D Earth heterogeneities poses a great challenge in calculating the Green's functions, because the existing 3D crustal velocity models are often inadequate in predicting high-frequency body waveforms at regional distances. To avoid the data deficiency and biases from inaccurate Green's functions, current approaches often involve joint inversions of long-period regional surface waves and short-period teleseismic P waves [Ford et al., 2012; Ni et al., 2010]. Such combination takes advantage of different frequency bands, but still face non-uniqueness problem in moment tensor inversions due to incomplete coverage of take-off angles and wave types.

In order to accurately determine the moment tensors of seismic events when the path structure is complex, approaches using 3D numerical Green's functions in the moment tensor inversions have been introduced [Covellone and Savage, 2012; Wang and Zhan, 2020]. Most models used to calculate the 3D Green's function can be categorized into travel-time-based and waveform-based tomographic models. Travel time tomographic models, such as the LLNL model by Simmons et al. [2012] and the SALSA3D model by Ballard et al. [2016], can predict the arrival times of body waves within errors of 3 seconds, so they can be used to precisely detect and locate small seismic events. However, these global travel time tomographic models are restricted by smoothing in the inversions and cannot accurately fit the seismic waveforms, especially in regions of complex structures. On the other hand, global and continental scale waveform tomographic models are promising in assimilating all available data and delivering the velocity models that can explain wiggles on seismograms [Bozdağ et al., 2016; Fichtner et al., 2009; C Tape et al., 2009]. But most of these models use long-period waveforms (T>17s globally or T>6s regionally) for inversion, partly because of the high computational cost, and partly due to the dependence of such sophisticated inversion on a good initial model at high frequencies. For specific areas that attract high research interest, adjoint tomographic inversions based on higher frequency seismic waveforms has been developed and implemented in source inversions [Jia et al., 2020b; Lee et al., 2014; Savage et al., 2014], but so far they are still limited by data coverage at high frequencies.

To avoid direct calculation of 3D Green's functions, the empirical Green's function (EGF) methods are also widely used in the monitoring, discrimination and relocation of seismic events, including nuclear explosions. Application of this type of method on nuclear tests takes advantage of the fact that they are often clustered within specific test sites. For example, all the North Korea nuclear tests so far are in the Punggye-ri test site, within a few km of each other [Wang and Hutko, 2018; Zhang and Wen, 2013; 2015]. As shown in Figure 1, the waveforms from the Feb 2013 and Jan 2016 North Korea tests recorded at the same station MDJ are highly similar to each other both at broadband and long periods (T>5s), despite that only the relatively simple long period recordings may be explained well by a regional velocity model. Such similarity at high frequencies is due to

the highly overlapping paths and common station terms. Using relative measurements, the path and site effects can be cancelled out in the source parameter estimations. Ni et al. [2010] used tectonic earthquakes to calibrate the path and site effects, thereby better fitting the waveforms in the moment tensor inversions. Lay et al. [1984] proposed the inter-correlation method to determine the source time function, yield, and depth of nuclear tests, taking another known nuclear test as reference event. It has been applied on source parameter estimation of North Korean nuclear explosions [Voytan et al., 2019]. Plourde and Bostock [2019] used relative amplitudes of body waves among a cluster of seismic events to constrain their moment tensors. Taking advantage of relative measurements, this type of EGF method greatly reduces moment tensor deviations caused by insufficient knowledge of the structure, but they can also introduce bias from a new assumption: the reference or calibration events are well understood, which is often not the case. Dahm [1996] avoided the assumption on a reference event in his relative moment tensor inversion algorithm, but he introduced an arbitrarily determined a priori constraint on moment tensor components, thus also facing the issue of biases and lack of uncertainty assessments. To reduce the deviation and bias of moment tensors, we need to incorporate Bayesian statistics in the relative moment tensor inversions with well assessed a priori information for appropriate estimation of posterior probability distributions.

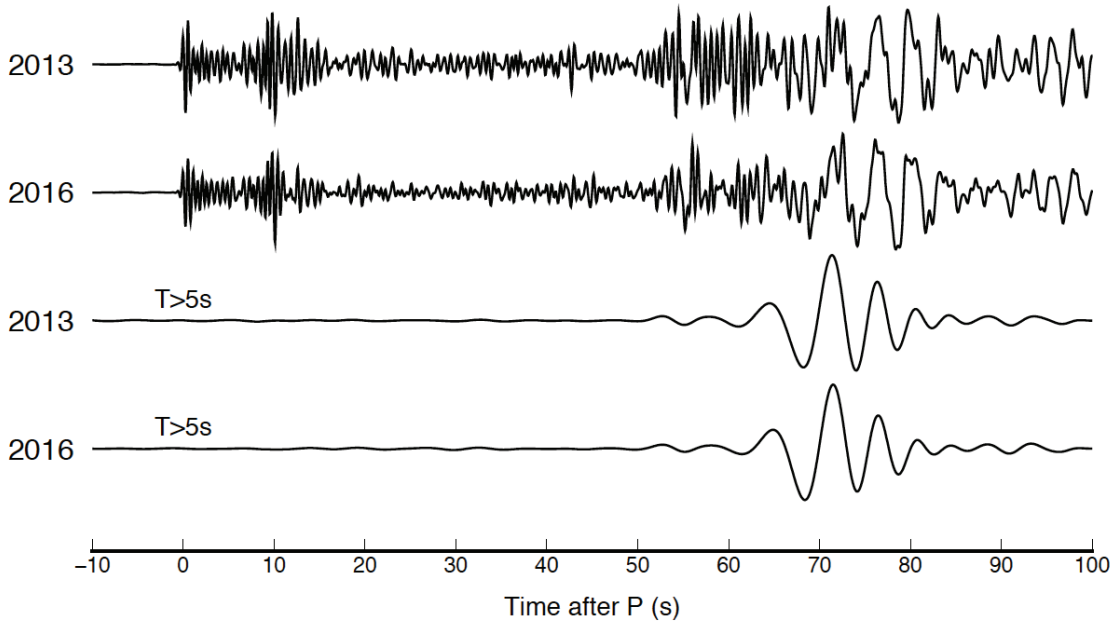

Figure 1. Waveform similarity of the Feb 2013 and Jan 2016 nuclear tests. *The similarities in both broadband (top two) and low-passed filtered (bottom two) waveforms recorded at station MDJ suggest largely shared path/site effects. Note that P waves are only visible at short periods. The epicentral distance is about 400km.*

In this study, we develop a new algorithm, named differential moment tensor inversion (diffMT), to determine the source parameters of nuclear tests in a Bayesian framework. In this method, we begin with using absolute measurements (i.e. waveforms) to invert for the individual moment tensors for a series of nuclear tests. The waveform-inverted results are used as a priori information for the second step, inversion of differential

measurements (i.e. relative amplitudes of body and surface waves) in a Bayesian framework. We apply the diffMT algorithm on four North Korea nuclear tests between 2009 and 2016. We compare our focal mechanism and moment magnitude results with traditional waveform inversion results, and analyze the explosion and tectonic release components of these nuclear tests. We further discuss the implications of our results on the explosion mechanisms of North Korea's nuclear tests.

3. METHODS, ASSUMPTIONS, AND PROCEDURES

Our diffMT method relies on refining the waveform-inversion-based prior distributions of moment tensors with additional differential measurements. Because data uncertainty due to path and site effects cancels out in differential measurements, the resulting model uncertainty should also decrease substantially. These should translate to more accurate estimates of yield and more robust discriminations for the nuclear tests. There are two steps involved in our method (Fig. 2). First, we use the generalized Cut-and-Paste (gCAP) waveform inversion method to constrain the individual moment tensors and their uncertainties. With these results as a priori information, we conduct Markov Chain Monte Carlo (MCMC) inversion on the differential measurements (the amplitude ratios for Pn/P, teleseismic P, Rayleigh and Love waves) in a Bayesian framework for the posterior probability density functions (PDF) of moment tensors.

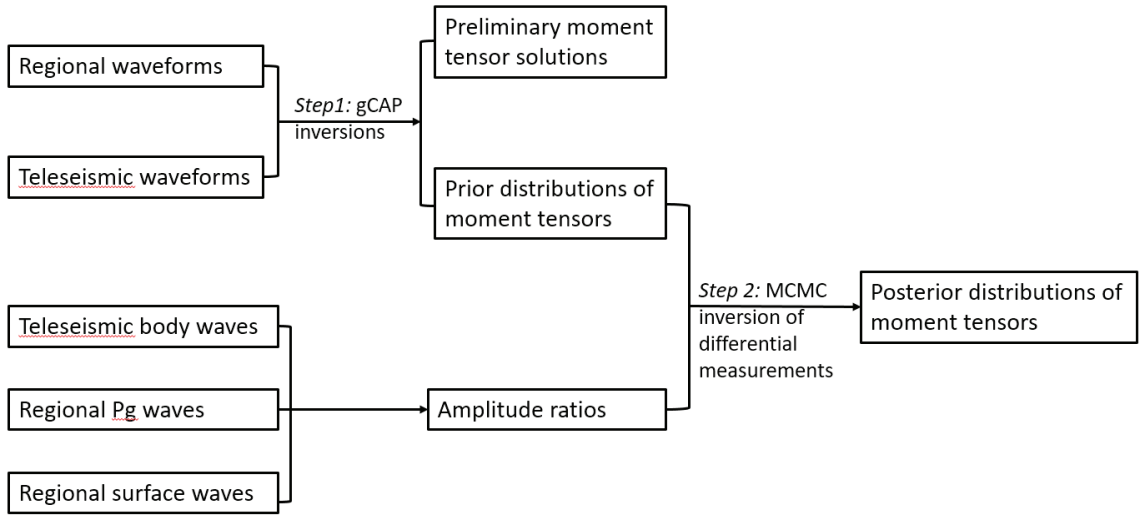

Figure 2. DiffMT method flowchart.

3.1 Generalized Cut-and-Paste inversion for prior information of moment tensors

Our first step is equivalent to most traditional moment tensor inversions and necessary for a Bayesian approach. In this study, we use gCAP3D [Zhu and Zhou, 2016] as our main driver for the inversion. Following the principles of the CAP methodology [Zhao and Helmberger, 1994; Zhu and Helmberger, 1996], gCAP3D breaks the seismograms into P- and S-/Surface-waves, and models them simultaneously but allowing different time shifts between observations and synthetics. The time shifts can accommodate

inaccuracies in the assumed velocity models and earthquake locations. The amplitude ratios between P- and S-/Surface-waves allow us to better constrain focal depths. We refer the readers to Zhu and Zhou [2016] for details of the inversion method. We further develop an automated inversion approach that can be applied in near real-time and produce a routine moment tensor catalog, with an iterative scheme with automatic data quality control [Wang and Zhan, 2020]. We demonstrated its accuracy and flexibility by applying it to small earthquakes in the Los Angeles region [Wang and Zhan, 2020].

The generalized CAP (gCAP) method allows full moment tensor inversions, without the double-couple constraint in earlier versions. We also improve the gCAP algorithm by jointly invert for the near-field and teleseismic data [Bai et al., 2020]. Bootstrapping can be used to estimate source parameter uncertainties in gCAP (e.g. [Jia et al., 2017; Zhan et al., 2012]), as prior constraints for the Bayesian inversions in Step 2. The calculation of Green's functions is based on the propagator matrix method with a plane wave approximation [Kikuchi and Kanamori, 1991] for the teleseismic body waves, and the frequency-wavenumber integration method [Zhu and Rivera, 2002] for regional surface waves. The source side velocity model is based on a combination of a 3-layer 1D elastic model [Ford et al., 2009] and the iasp91 model [Kennett et al., 1995].

3.2 Bayesian DiffMT using waveform amplitude ratios.

In this step, we search the moment tensor model space based on the prior PDFs from the first step for solutions that best explain the differential measurements. Due to the clustering source locations of nuclear explosions, we can extract differential measurements from various type of waves. In this study, we take amplitude ratios of regional Pn/P, teleseismic P, regional Rayleigh and Love waves from two events at the same stations to cancel out the path and site effects. This is because the recorded seismic waves can be represented by

$$u_1(\boldsymbol{x},t) = M_{ij}^1 * G_{ij}(\boldsymbol{x},t) * S_1(t) * r(\boldsymbol{x}), \quad (1)$$

$$u_2(\boldsymbol{x},t) = M_{ij}^2 * G_{ij}(\boldsymbol{x},t) * S_2(t) * r(\boldsymbol{x}), \quad (2)$$

where 1 and 2 denote the two events, M_{ij} is the full moment tensor, G_{ij} is the Green's function, S is the source time function, and r is the station amplification term. If we assume that the event source durations for nuclear tests are in general much shorter than the seismic wave period (e.g., T~1s) used in inversions, then the small differences in amplitudes and waveforms are almost only sensitive to differences in source processes (e.g., depth, yield, radiation pattern), not the common path/site effects. For the body waves, including the regional Pn/P phase and teleseismic P waves, the amplitude ratios are simply reduced to the radiation pattern ratios. In this case, the calculation of theoretical amplitude ratios can be simplified to the function of take-off angle and azimuth with ray theory implemented in a layered elastic media [Dahm, 1996]. For vertical component P waves of an event pair recorded at the same station, we cut the time window 3s after the P arrival for regional P waves, and 5s for the teleseismic waves, and cross-correlate the waves of two events to measure the amplitude ratios. We choose our data and error to be the mean and half deviation of the two different measurements,

$$ln(A^1) = \frac{\int u(\tau - t)v(\tau)d\tau}{\int v^2(\tau)d\tau} \quad (3)$$

$$ln(A^2) = \frac{\int u^2(\tau)d\tau}{\int u(\tau - t)v(\tau)d\tau} \quad (4)$$

where *u(t)* and *v(t)* are the waves segments of two events after cross-correlation. The term $ln(A^1)$ indicates the amplitude ratio *u/v* taking v^2 as the denominator, while $ln(A^2)$ is the inverse of *v/u* taking u^2 as the denominator. Theoretically, the amplitude ratios do not depend on the frequency band we are using, but they can vary in practice. Therefore, we also measure amplitude ratios in different frequency bands, and count the differences in the data errors.

While the amplitudes for body waves are straightforward to compute, the surface wave amplitudes have a more complex dependence on the moment tensors and depths. We introduce an analytical form of the surface wave radiation patterns for the shallow sources, and then explore the constraints on moment tensors components from the DiffMT inversion. For nuclear explosions, the source depths are very shallow, resulting in surface wave eigenfunction terms

$$l_2(h) = \mu \frac{dl_1}{dz}\Big|_h = 0, \quad (5)$$

$$r_3(h) = \mu \left(\frac{dl_1}{dz} - kr_2\right)\Big|_h = 0, \quad (6)$$

$$r_4(h) = 0. \quad (7)$$

The excitation of Rayleigh and Love waves by a source with moment tensor M is given [Aki and Richards, 2002] by

$$u^{Rayleigh}(\boldsymbol{x}, \omega) = \boldsymbol{G^R}[U_1 + U_2 cos2\phi + U_3 sin2\phi], \quad (8)$$

$$u^{Love}(\boldsymbol{x}, \omega) = \boldsymbol{G^L}[U_2 sin2\phi - U_3 cos2\phi], \quad (9)$$

where $\boldsymbol{G^R}$ and $\boldsymbol{G^L}$ are given by

$$\boldsymbol{G^R}(\boldsymbol{x}; h, \omega) = \sum_n \frac{k_n r_1(h)}{8cUI_1} \sqrt{\frac{2}{\pi k_n r}} \exp\left[i\left(k_n r + \frac{\pi}{4}\right)\right][r_1(z)\hat{\boldsymbol{r}} + ir_2(z)\hat{\boldsymbol{z}}], \quad (10)$$

$$\boldsymbol{G^L}(\boldsymbol{x}; h, \omega) = \sum_n \frac{ik_n l_1(h)}{8cUI_1} \sqrt{\frac{2}{\pi k_n r}} \exp\left[i\left(k_n r + \frac{\pi}{4}\right)\right] l_1(z)\hat{\boldsymbol{\phi}}, \quad (11)$$

in which μ is the shear modulus and k_n is the nth root of the wavenumber. The radiation pattern coefficients, U_1, U_2, U_3 are given by

$$U_1 = \frac{1}{2}(M_{xx} + M_{yy}) - \left(1 - \frac{2\beta^2}{\alpha^2}\right) M_{zz}, \quad (12)$$

$$U_2 = \frac{1}{2}(M_{xx} - M_{yy}), \quad (13)$$

$$U_3 = M_{xy}. \quad (14)$$

Given two nuclear explosions E1 and E2 that are buried shallow and closely located, these events share similar $\boldsymbol{G^R}$ and $\boldsymbol{G^L}$, hence these terms can be cancelled out by calculating the amplitude ratios. The analytical form of Rayleigh and Love wave amplitude ratios would simply be

$$\boldsymbol{A^R}|_{\frac{E1}{E2}} = \frac{(U_1 + U_2 cos2\phi + U_3 sin2\phi)|_{E1}}{(U_1 + U_2 cos2\phi + U_3 sin2\phi)|_{E2}}, \quad (15)$$

$$\boldsymbol{A^L}|_{\frac{E1}{E2}} = \frac{(U_2 sin2\phi - U_3 cos2\phi)|_{E1}}{(U_2 sin2\phi - U_3 cos2\phi)|_{E2}}. \quad (16)$$

which are only functions of moment tensors M_{E1}, M_{E2},, Vp/Vs ratios β/α, and station azimuth ϕ, suggesting that we can take away the path effects simply by calculating amplitude ratios of surface waves. Given the information of elastic media and station information, the amplitude ratios of surface waves are nonlinear functions of moment tensor components. Measurement of the surface wave amplitude ratios and errors is similar to that of body waves, and we choose the time window to be 70s after the predicted group arrival assuming wave velocities of 3.0 and 3.2 km/s for Rayleigh and Love waves, respectively. The Rayleigh waves are different from other wave types as they are observed at two components, radial and vertical. Hence we consider the difference in measurements of these two components in the data error assessment.

We use the Metropolis-Hasting Markov Chain Monte-Carlo (MCMC) method to sample the prior PDFs of moment tensors from Step 1, and estimate the posterior PDFs of two events based on fitting of the amplitude ratios of body and surface waves. The MCMC algorithm follows a Bayesian framework that produces model error from data error of differential measurements (amplitude ratios) and the a priori information [Tarantola, 2005]. In addition to the a priori information of 6 independent moment tensor components (Mrr, Mtt, Mpp, Mrt, Mrp, Mtp), we incorporate the gCAP moment magnitude distribution into the prior constraints to avoid moment trade-off of two events. We generate 24 Markov Chains from random initial samples, and eventually keep 1/3 of those chains to avoid being trapped in local minima. In each Markov Chain step, we propose new models through sampling of one of the nonlinear parameters while keeping the other nonlinear parameter at their current values [Jia et al., 2020a], which ensures an overall high acceptance rate, and therefore improves the convergence efficiency of the MCMC inversion.

4. RESULTS AND DISCUSSION

We apply our diffMT algorithm on the event pairs among the four North Korea nuclear tests on May 2009, Feb 2013, Jan 2016 and Sep 2016, respectively. We collect the regional (within epicentral distance of 15°) and teleseismic (epicentral distance between 30° and 90°) waveforms of the Global Seismic Network (GSN) and the International Federation of Digital Seismograph Networks (FDSN) stations. We apply gCAP inversion to the four nuclear tests by jointly inverting local and teleseismic waves. We include regional surface waves in the 10-50s period band, and teleseismic P waves in the 1-2s period band. Short-period regional P waves are not included here because existing

velocity models cannot predict the waveform wiggle shapes. Due to the poor constraints on the centroid depths, the inversions are conducted at a fixed depth of 0.6 km, similar to the estimations from Voytan et al. [2019]. Fig. 3 shows the inversion results for the four tests. Both the regional and teleseismic waveforms are fit well. We estimate ~70% isotropic component and moment magnitudes between 4 and 5 for all these events, generally consistent with other moment tensor inversion results which isotropic component ranging from 50% to 80% [Cesca et al., 2017; Chiang et al., 2018; Ford et al., 2009].

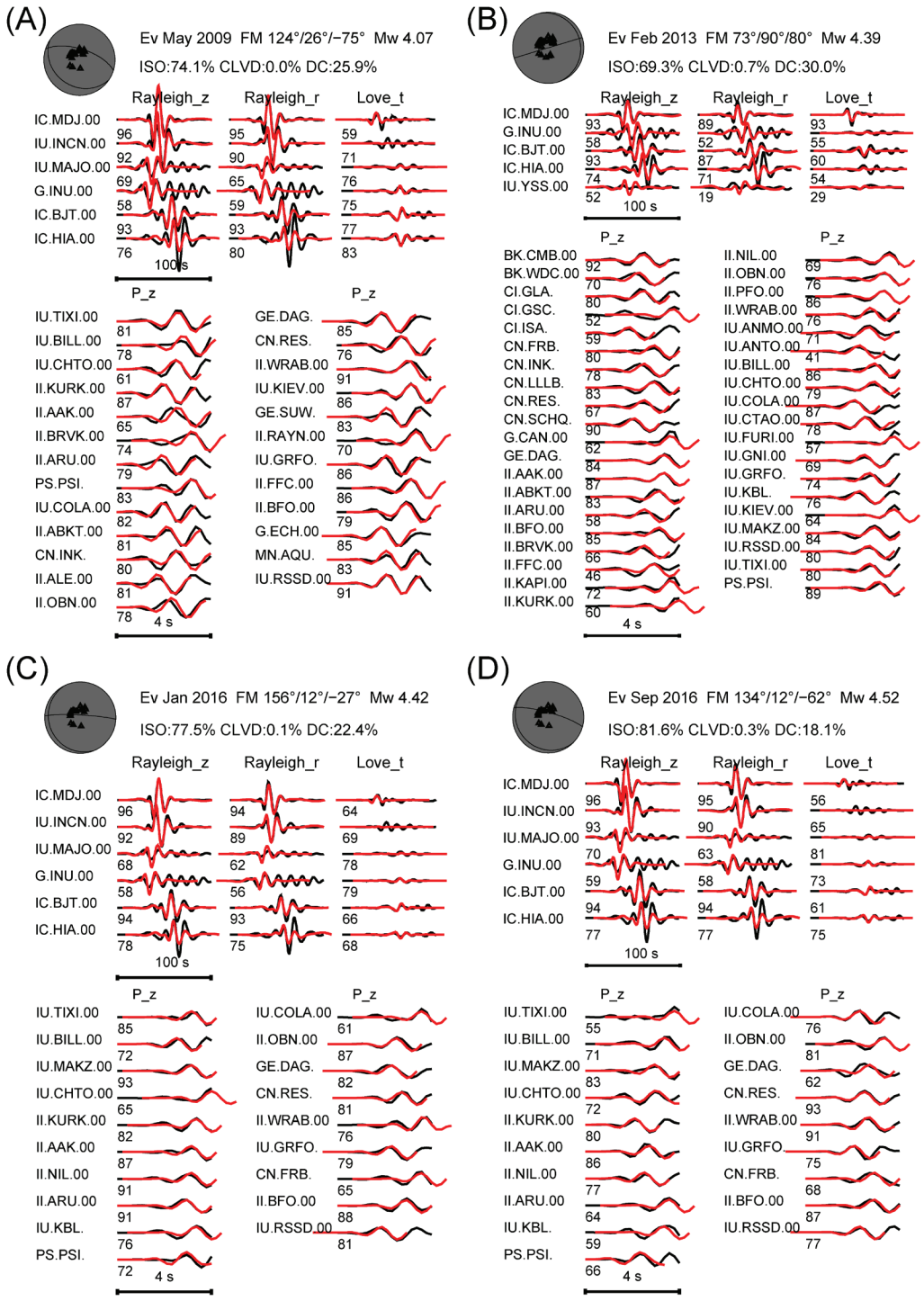

Figure 3. gCAP inversion results for the 4 studied North Korea nuclear explosions on (A) May 2009, (B) Feb 2013, (C) Jan 2016 and (D) Sep 2016, respectively. *The black and red lines indicate data and synthetic waveforms, respectively. The numbers leading the waveforms are the cross-correlation coefficients between data and synthetics.*

To estimate the uncertainty of the gCAP moment tensor solutions, we apply a cut-half bootstrapping approach in which we randomly remove half of our data and run the gCAP inversion. We repeated this process 200 times, and then calculated the standard deviation of the obtained moment tensor components for an approximation of the model error. The distributions of the moment tensors for 4 events shown in Fig. 4 suggest that all the moment tensor components have large uncertainties. Particularly, the moment magnitudes and fractions of the isotropic component in focal mechanisms are not well constrained. In contrast to the insights simply from the optimal solutions, the addition of model uncertainties makes it hard to discriminate the events as explosions and assess the yields in confidence.

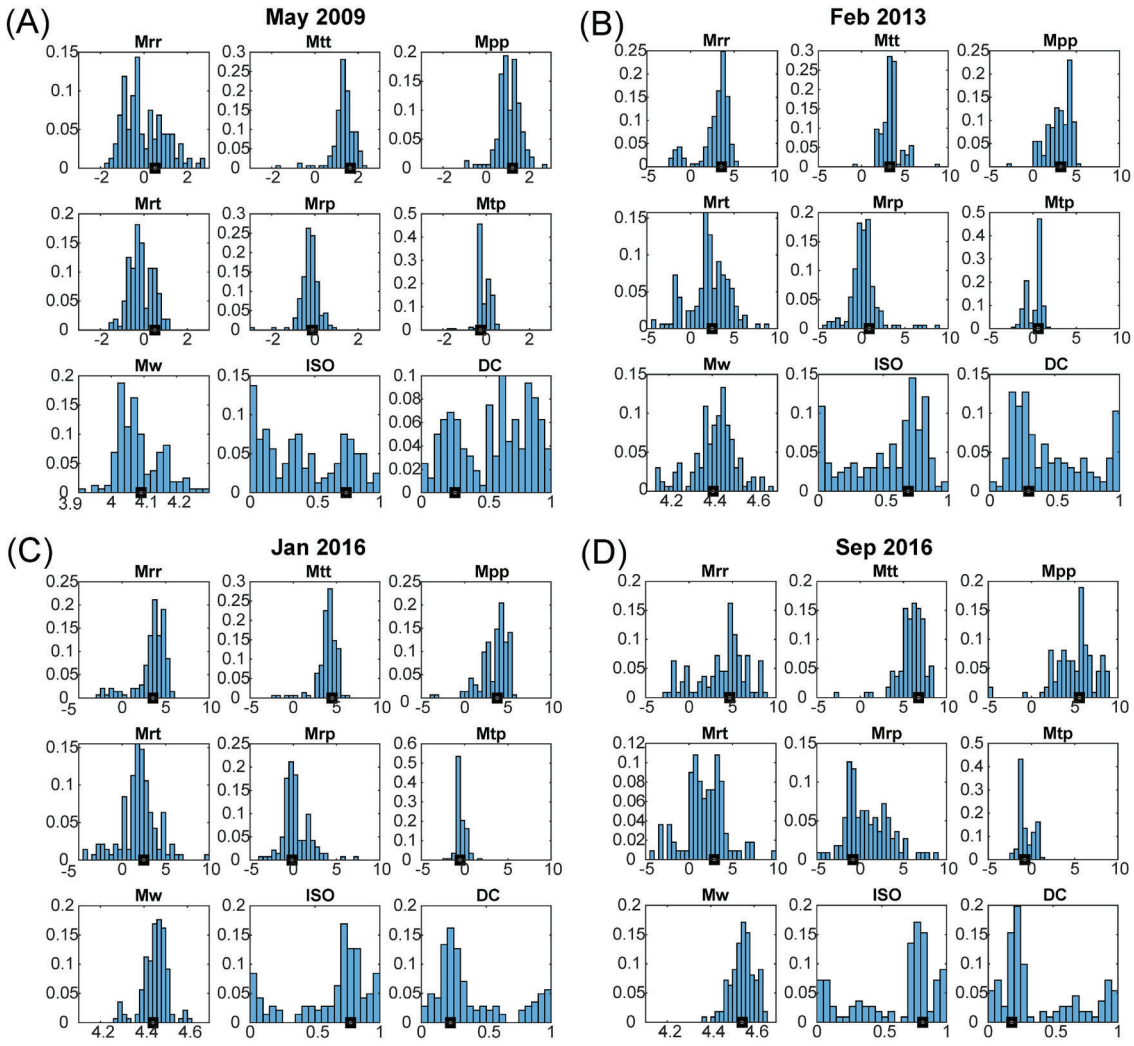

Figure 4. Distribution of gCAP source parameters including moment magnitude components, moment magnitude, isotropic and double-couple proportion from bootstrapping sampling. *Results for 4 Nuclear tests are shown in panels A-D, respectively.*

We break the 4 events into 6 event pairs, and use the gCAP moment tensor solutions as a priori information for the second step of the diffMT inversion, where we add new constraints from body and surface wave amplitude ratios and apply Metropolis-Hasting MCMC to assess the posterior PDFs. Taking the event pair including the Feb 2013 and the Jan 2016 events as an example, the amplitude ratios of regional P, teleseismic P, and the Rayleigh and Love waves are measured through cross-correlations (Fig. 5). In the differential data measurement, we filter the P waves between 0.5~2.0 Hz, and filter the Rayleigh/Love waves between 0.05~0.2 Hz, respectively. The body waves and surface waves for the two events show high similarity, suggesting robust measurements of the amplitude ratios. These differential measurements show a clear azimuthal dependence, suggesting azimuthally varying radiation patterns, which are presumably caused by focal mechanism differences. We do not account for the variations of surface reflections caused by 3D topography over the source locations, which also results in azimuthally dependent amplitude variations. A recent numerical study [Avants, 2014] suggests that the fluctuations in surface reflection amplitudes are not significant using realistic surface topography. Nevertheless, the influence of the surface topography on amplitude ratio variations should be further studied, as the errors of source locations could bring uncertainty in such quantification.

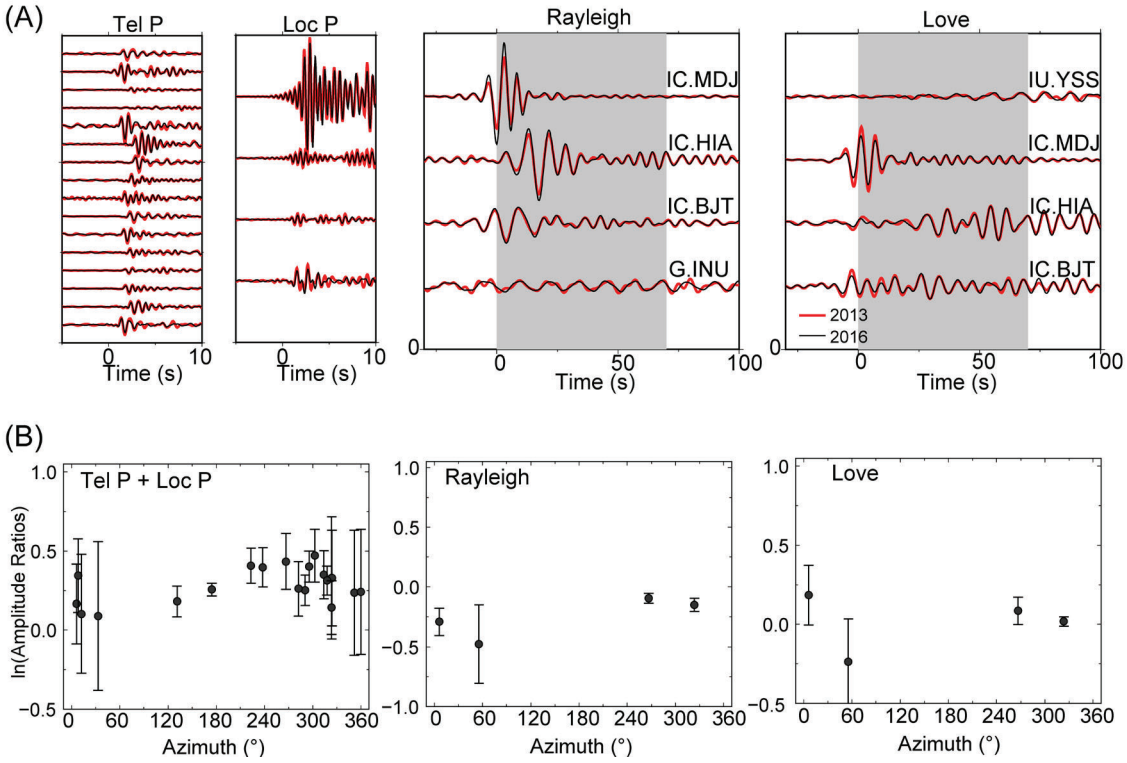

Figure 5. Measurements of amplitude ratios between the Feb 2013 and Jan 2016 events. *(A) Cross-correlations for teleseismic P (TEL P), regional P (Loc P), Rayleigh and Love waves, respectively. (B) Amplitude ratios for P, Rayleigh and Love waves as a function of the station azimuth. The y axis is in natural logarithmic scale. The standard deviation errors are shown with the error bars.*

Using these measured amplitude ratios, the diffMT inversion results for the Feb 2013 and the Jan 2016 events are shown in Fig. 6. The final diffMT moment tensor solution, defined as the mean of the diffMT moment tensor ensemble, are not too different from the gCAP solution (Gaussian approximations to the non-Gaussian original bootstrapping distributions), but the additional constraints from the body and surface wave amplitude ratios significantly tightened some of the posterior PDFs (Fig. 6A). Improvements of PDFs are substantial for some moment tensor components but insignificant for others, presumably because the variations of certain components (like Mrt and Mrp) only changes the DC/CLVD orientations which are relatively minor to the isotropic components. Compared with the gCAP solution, the diffMT moment tensors substantially improve the fittings of the amplitude ratios (Fig. 6B). We decompose the gCAP and diffMT solutions into the isotropic (ISO), double couple (DC) and CLVD components (Fig. 6C). For both the diffMT and the gCAP solutions, the tectonic release (DC) components are both high angle dip-slip mechanisms. The strike and dip angles after diffMT inversion, however, are slightly different from the gCAP solution. The DC moments for both events decreased after the inversion, preferring an explosive focal mechanism.

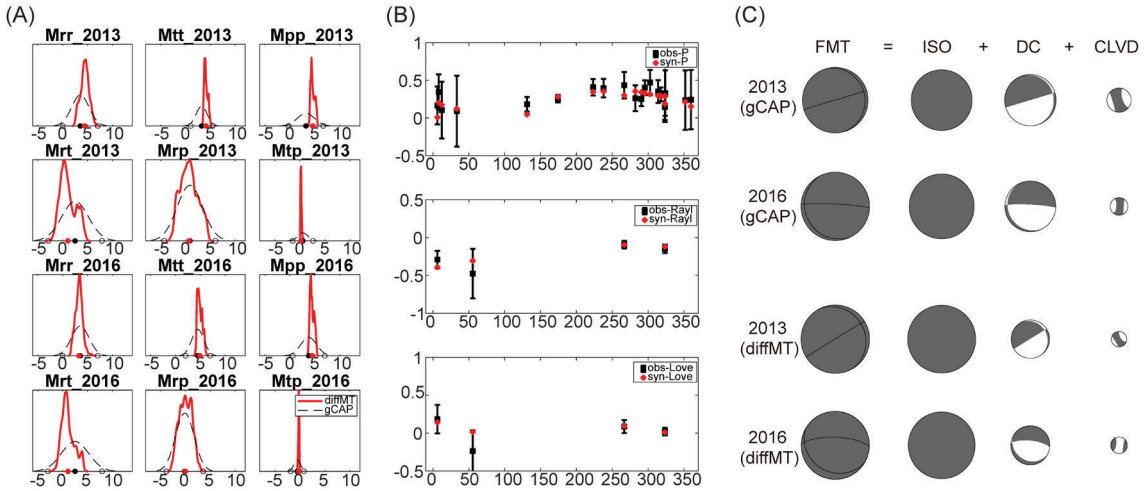

Figure 6. DiffMT inversion results for the event pair of the Feb 2013 and Jan 2016 tests. *(A) The prior (dashed black lines) and the diffMT posterior (red lines) PDFs of the moment tensor solutions of the two events. The prior (gCAP) is from Gaussian fitting of bootstrapping uncertainties. Black and red dots indicate the gCAP and diffMT solutions, respectively. (B) Amplitude ratio fittings for the diffMT solution. Black squares and red dots show the amplitude ratio data and predictions from the moment tensor models, respectively. (C) Moment tensor decompositions for the gCAP and diffMT solutions. The sizes of the beachballs are proportional to the corresponding magnitudes.*

We apply the diffMT inversion on all 6 event pairs. Fig. 7 shows a chart of the diffMT solutions for all 4 events from different event pairs. We found that three events of them, the Feb 2013, the Jan 2016 and the Sep 2016 Nuclear tests, form a self-consistent group, that is, the moment tensor solution of each individual event does not depend on the other

event it pairs with. Considering that the differential measurements for the different event pairs are independent, the consistent moment tensor solutions illustrate the effectiveness of the diffMT method. The exception is the 2009 Nuclear test. For other Nuclear tests, being paired with the 2009 event leads to similar proportion of ISO/DC components yet different DC component solutions (Fig. 7A). This inconsistency could be due to the relatively poor quality of the amplitude ratio measurements (Fig. 7B) caused by the small magnitude (Mw 4.1) and low signal-to-noise ratio of the 2009 Nuclear test. The CLVD components are trivial, suggesting that the collapse and tensile cracking are not significant during these nuclear tests.

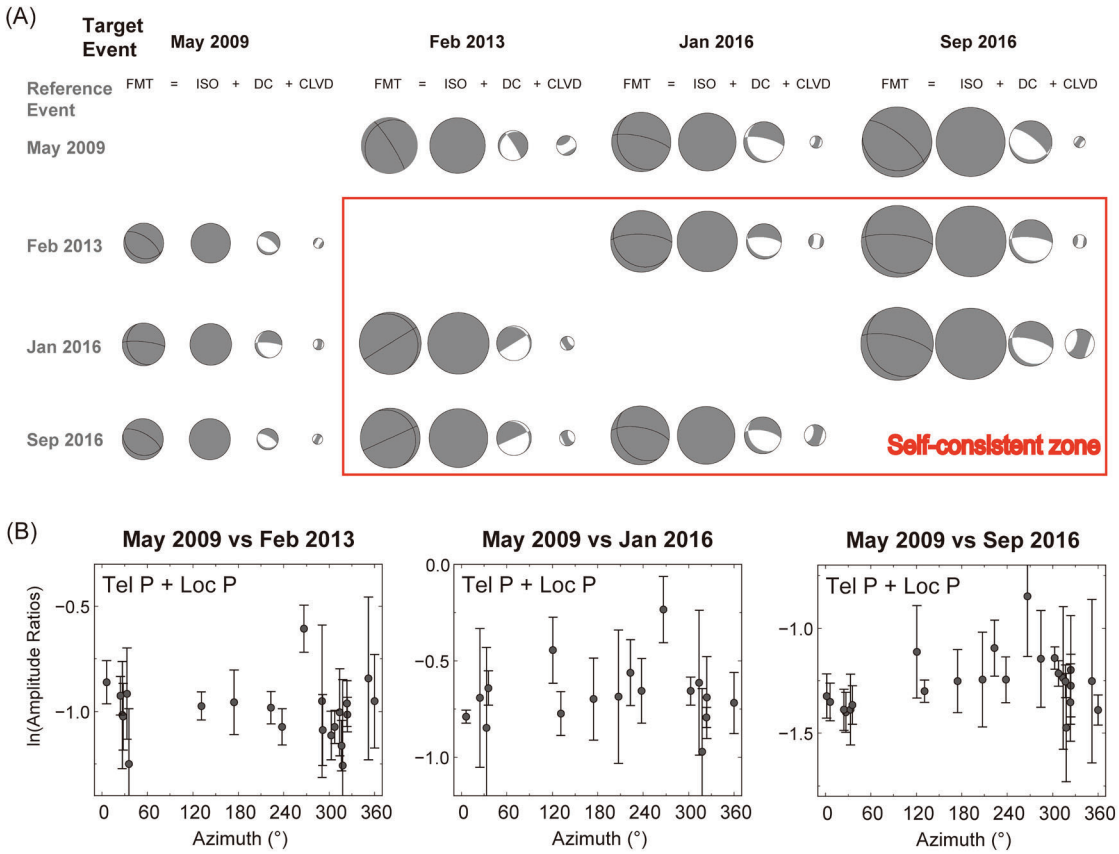

Figure 7. Consistency analysis of the diffMT inversion for all possible event pairs. *(A) Moment tensor solutions for each event (columns) from different paired events (rows). Ideally, the moment tensor solutions of same individual event from different pairs (each column) are expected to be consistent. The red box denotes a self-consistent zone among the Feb 2013 and two 2016 nuclear tests. (B) P wave amplitude ratios for event pairs including the May 2009 nuclear test.*

The prior and posterior PDFs of moment magnitude and proportions of ISO, DC and CLVD components are shown in Fig. 8. For all four events, the posterior PDFs are significantly narrower and right-shifted compared with the prior PDFs (Fig. 8), suggesting tighter constraints on the focal mechanism components and the moment magnitudes. In particular, the proportion of the isotropic/double-couple components are

much better resolved (Fig. 9). Taking the Feb 2013 Nuclear test as an example, the ISO components are now centered above 90%, and are almost entirely above 50%. Yet the likelihood of 90% isotropic moment tensor is not very high based on the gCAP PDFs. The narrower moment magnitude PDFs, especially for the 2009 and 2013 events of smaller magnitudes, suggest that they are also better constrained after the diffMT inversion. The ISO components are significantly more dominating after the inversions, strongly suggesting explosive focal mechanisms. Moreover, diffMT inversions make it much easier to estimate and compare the energy release of these nuclear tests. This is because differences in moment tensor are constrained by differential measurements and are potentially better resolved than the absolute values. Therefore, the additional constraints from amplitude ratios provide us with confidence in explosive event discrimination and yield comparison.

Our application of the diffMT inversion on the North Korea nuclear tests suggests differential measurements provide additional constraints on moment tensors. Although the absolute amplitude information for regional surface waves and teleseismic P waves have been used in the gCAP waveform inversion, the patterns of amplitude ratios are not captured by traditional inversions. This can be illustrated by the data fittings of the diffMT and gCAP solutions. Taking the Feb 2013 North Korea nuclear test as an example, the fittings to regional and teleseismic waveforms for the gCAP and diffMT solutions are very similar with each other (Fig. 10), suggesting the waveforms' misfit can hardly distinguish the two moment tensor solutions, reflecting the non-uniqueness problem. In contrast, the diffMT solution fits amplitude ratios significantly better than the gCAP solution (Fig. 10). This is because the absolute amplitude information in the waveforms are largely influenced by the path and site effects, and the attempts to fit them assuming a simple structural model cause large uncertainty in the waveforms inversions.

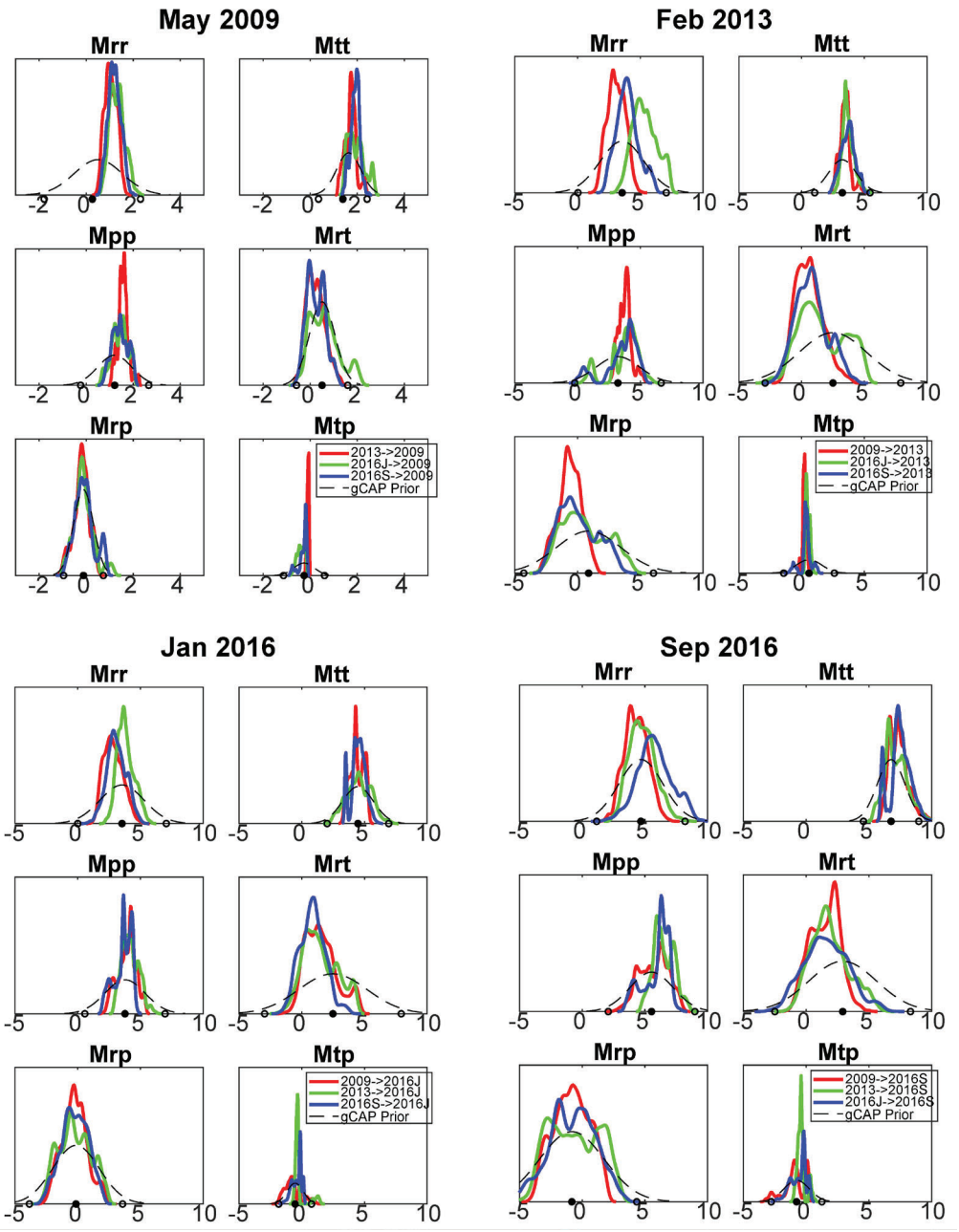

Figure 8. gCAP prior (dashed black lines) and diffMT posterior (solid lines) PDFs of 6 moment tensor components for 4 studied events. *Solid lines in different colors indicate the posterior PDFs derived with different pairing events.*

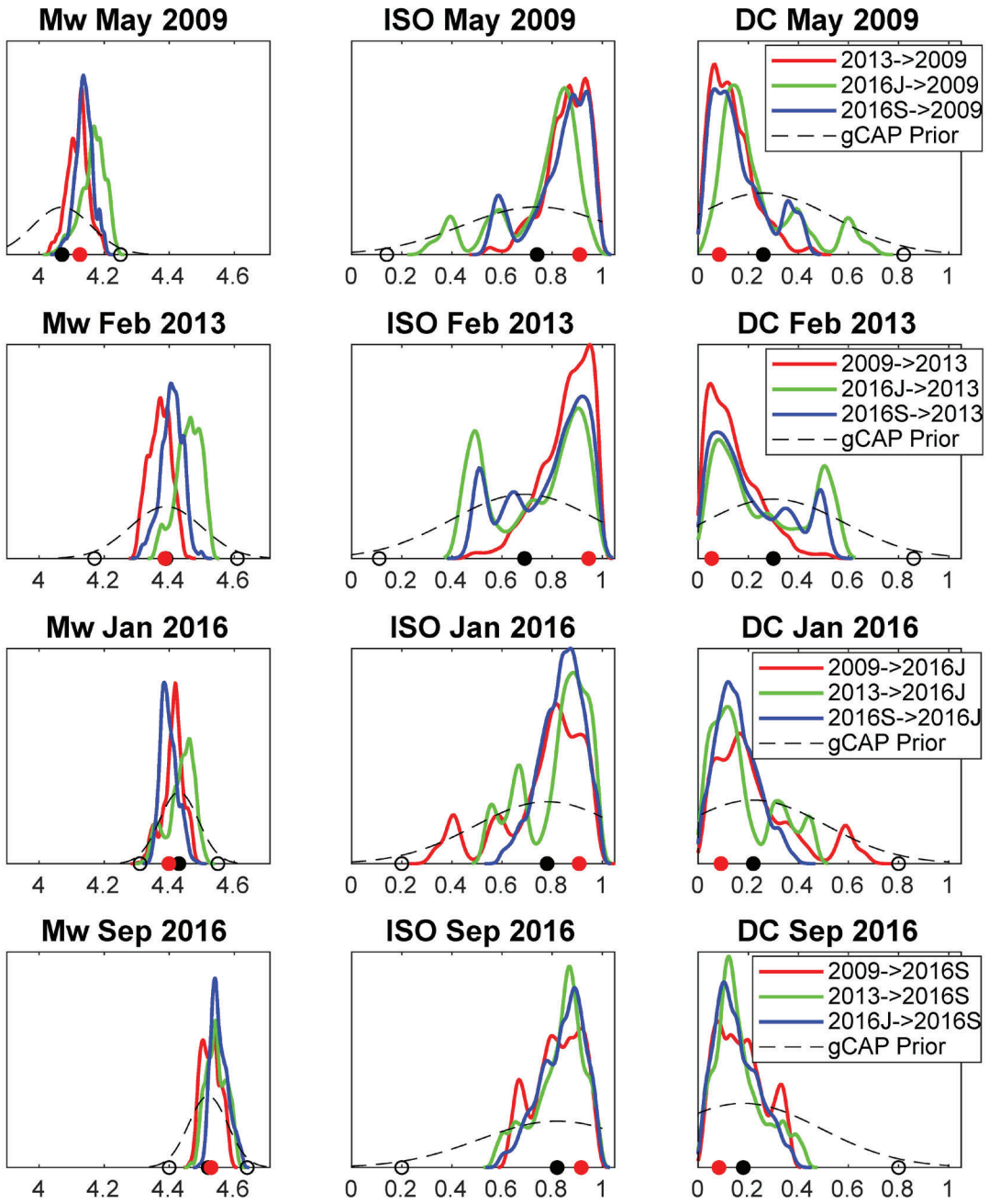

Figure 9. gCAP prior (dashed black lines) and diffMT posterior (solid lines) PDFs for the source parameters include moment magnitude, isotropic and double-couple proportions. *Lines of different colors are also posterior PDFs obtained with different pairing events.*

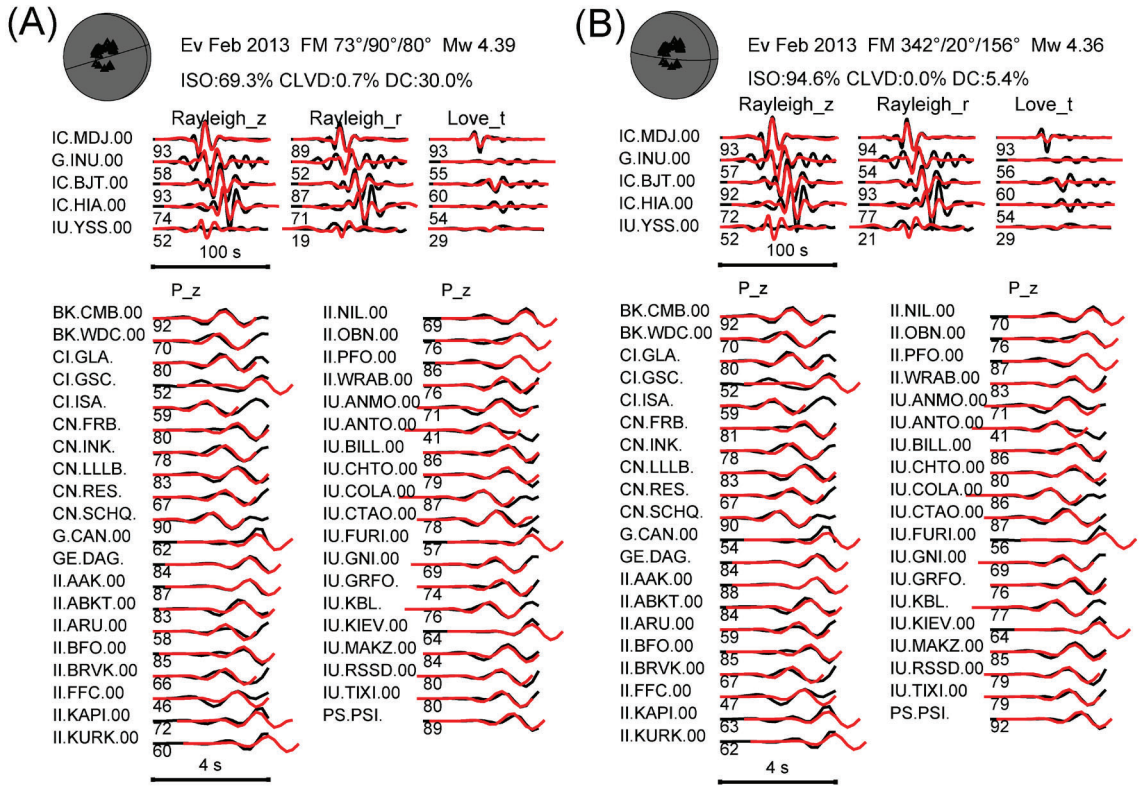

Figure 10. Comparison of (A-B) waveform fittings and (C-D) amplitude ratio fittings for the gCAP and diffMT solutions. *The waveform fitting difference is hardly observable, suggesting that the moment tensor difference of these two solutions can't be resolved by the gCAP waveform inversion. The amplitude ratio fitting improvement for the diffMT solution is substantial, indicating tighter constraints on the moment tensors from differential measurements.*

Source parameter inversion that uses relative measurements to avoid path and site effects have been developed and implemented in various studies [Dahm, 1996; Plourde and Bostock, 2019; Voytan et al., 2019; Xu et al., 2020]. Compared with these methods, our diffMT algorithm uses the two-step approach that allows us to jointly incorporate the waveforms' information together with the amplitude ratio constraints, and quantitatively convert the data errors into moment tensor uncertainties through a Bayesian framework. However, our calculations of body wave amplitude ratios rely on ray theory using a simple layered crustal model, and the influence of structural heterogeneities on the ray parameter is not considered. We found that the influence of depth phases on the amplitude ratios are insignificant in the 1D case, but we have not assessed the impact of 3D surface topographic reflections. All of these suggest that 3D structures may still bias our inversion results, suggesting that full numerical wavefield simulations in more realistic structure are required in the future.

Although the diffMT solutions for every studied event are generally consistent for different pairs, we can still observe differences between different event pairs for certain components, such as the moment magnitude and the Mrr component for the Feb 2013 event (Fig. 8-9). The posterior PDFs have some overlapping ranges with each other,

suggesting solutions within the overlapped ranges are capable to fit the independently measured amplitude ratios from different pairs. This illuminates the value of our diffMT in the Bayesian framework: introducing differential measurements to eliminate the solutions which are assumed "possible" from the absolute measurements. The differential measurements themselves do not provide constraints on the absolute value of moment magnitude: a simple conceptual test is that we can fit the amplitude ratios equally well with the seismic moments of all events multiplied by the same value. But the extra constraints from differential measurements can eliminate solutions that are hardly distinguishable for traditional gCAP inversions, thus making the posterior PDFs tighter and errors lower. The reason why the maximum likelihood solutions for different event pairs are diverging to different directions (e.g. Mw for the Feb 2013 test) can be due to the varying data and modeling errors. Existence of these errors make one model group fit the 2009-2013 differential measurements but not fit the 2016-2013 amplitude ratios, while turning another model group in an opposite way. The other model group corresponding to the overlapping part of the posterior PDFs fits both the 2009-2013 and the 2016-2013 pairs well. This difference in model groups results in the two posterior PDFs from two event pairs diverging to opposite directions, but as long as they have overlapping model space, they are not contradicting with each other. The agreement of other parameters for our solution from different event pairs suggest that these parameters are not sensitive to the data and modeling errors of the differential measurements.

We merge the diffMT moment tensor ensembles of each single nuclear test from different event pairs to obtain the overall solution (Table 1). The results show that the explosive source component dominates the four nuclear tests in North Korea. The proportions of the isotropic components are all around 90% (Table 2), compared to gCAP estimates of around 70%, or some other traditional moment tensor inversion solutions of 50%-60% [Cesca et al., 2017; Ford et al., 2009; Vavryčuk and Kim, 2014]. The moment magnitudes of these four events are estimated to be 4.12, 4.39, 4.40, and 4.53 respectively. Double couple components are mostly dip-slip normal faulting events, and the steep dip angle is common in correspondence to dominant positive isotropic sources [Cesca et al., 2017]. The DC orientations are also consistent with the DC terms of North Korea explosions resolved by Ford et al. [2009] and Cesca et al. [2017]. But similar to the bottlenecks of most moment tensor inversion, our diffMT algorithm only resolves point source moment tensors, therefore does not distinguish the detailed energy release process, such as the temporal sequence and location difference of the explosions, tectonic releases, and collapses. Further investigations of time-dependent source processes are needed for large and complicated nuclear explosions, such as the Sep 2017 North Korea nuclear test (M 6.3).

Table 1. Moment tensor solutions for the 4 studied North Korea nuclear tests.

	Mrr (10^{22} dyne-cm)	**Mtt (10^{22} dyne-cm)**	**Mpp (10^{22} dyne-cm)**	**Mrt (10^{22} dyne-cm)**	**Mrp (10^{22} dyne-cm)**	**Mtp (10^{22} dyne-cm)**
May 2009	1.190	1.863	1.473	0.363	-0.129	-0.272
Feb 2013	4.137	3.614	3.678	1.014	0.008	0.356
Jan 2016	3.253	4.495	3.904	1.288	-0.234	-0.439
Sep 2016	4.959	7.335	6.049	1.660	-0.737	-0.669

Table 2. Comparison of isotropic, double-couple and CLVD proportions of 4 studied North Korea nuclear tests for gCAP and DiffMT solutions.

gCAP/diffMT	**Mw**	**ISO**	**DC**	**CLVD**
May 2009	4.07/4.12	74.1%/91.0%	25.9%/8.4%	0.0%/0.6%
Feb 2013	4.39/4.39	69.3%/94.6%	30.0%/5.4%	0.7%/0.0%
Jan 2016	4.42/4.40	77.5%/90.8%	22.4%/9.1%	0.1%/0.1%
Sep 2016	4.52/4.53	81.6%/91.6%	18.1%/8.2%	0.3%/0.2%

5. CONCLUSIONS

We developed a new method called differential moment tensor (DiffMT) inversion that can take the amplitude ratios of seismic phases from two co-located events to refine their moment tensors. The method starts with a conventional moment tensor inversion for the prior moment tensor information both events, followed by running MCMC inversion of the differential amplitudes of regional/teleseismic P waves and regional surface waves for the refinements. Application of the diffMT inversion on four North Korea nuclear tests between 2009 and 2016 reduced the uncertainty of the moment tensor components. Moment tensors of all four studied nuclear tests are dominated by ~90% isotropic components, substantially improved compared with some conventional inversion results of 50%~60% with large uncertainties. The associated tectonic release components are small but nontrivial dip-slip mechanisms. The inversion also substantially improves the estimation of isotropic components and moment differences between events, providing tighter constraints on nuclear test discrimination and yield estimation.

REFERENCES

Aki, K. and P. G. Richards (2002), Quantitative seismology, Sausalito, CA, University Science Books.

Alvizuri, C. and C. Tape (2018), Full moment tensor analysis of nuclear explosions in North Korea, Seismol. Res. Lett., 89(6), pp. 2139-2151.

Avants, M. (2014), Effects of near-source heterogeneity on wave fields emanating from crustal sources observed at regional and teleseismic distances, Doctoral dissertation, UC Santa Cruz, CA.

Bai, Q., S. Ni, R. Chu, and Z. Jia (2020), gCAPjoint, A Software Package for Full Moment Tensor Inversion of Moderately Strong Earthquakes with Local and Teleseismic Waveforms, Seismological Society of America, 91(6), pp. 3550-3562.

Ballard, S., J. R. Hipp, M. L. Begnaud, C. J. Young, A. V. Encarnacao, E. P. Chael, and W. S. Phillips (2016), SALSA3D: A Tomographic Model of Compressional Wave Slowness in the Earth's Mantle for Improved Travel-Time Prediction and Travel-Time Prediction UncertaintySALSA3D: A Tomographic Model of Compressional Wave Slowness in the Earth's Mantle, Bulletin of the Seismological Society of America, 106(6), pp. 2900-2916.

Bozdağ, E., D. Peter, M. Lefebvre, D. Komatitsch, J. Tromp, J. Hill, N. Podhorszki, and D. Pugmire (2016), Global adjoint tomography: first-generation model, Geophysical Journal International, 207(3), pp. 1739-1766.

Cesca, S., S. Heimann, M. Kriegerowski, J. Saul, and T. Dahm (2017), Moment tensor inversion for nuclear explosions: What can we learn from the 6 January and 9 September 2016 nuclear tests, North Korea?, Seismol. Res. Lett., 88(2A), pp. 300-310.

Chiang, A., G. A. Ichinose, D. S. Dreger, S. R. Ford, E. M. Matzel, S. C. Myers, and W. Walter (2018), Moment Tensor Source-Type Analysis for the Democratic People's Republic of Korea–Declared Nuclear Explosions (2006–2017) and 3 September 2017 Collapse Event, Seismol. Res. Lett., 89(6), pp. 2152-2165.

Covellone, B. M. and B. Savage (2012), A quantitative comparison between 1D and 3D source inversion methodologies: Application to the Middle East, Bulletin of the Seismological Society of America, 102(5), pp. 2189-2199.

Dahm, T. (1996), Relative moment tensor inversion based on ray theory: theory and synthetic tests, Geophysical Journal International, 124(1), pp. 245-257.

Ekström, G., M. Nettles, and A. Dziewoński (2012), The global CMT project 2004–2010: Centroid-moment tensors for 13,017 earthquakes, Physics of the Earth and Planetary Interiors, 200, pp. 1-9.

Fichtner, A., B. L. Kennett, H. Igel, and H.-P. Bunge (2009), Full seismic waveform tomography for upper-mantle structure in the Australasian region using adjoint methods, Geophysical Journal International, 179(3), pp. 1703-1725.

Ford, S. R., D. S. Dreger, and W. R. Walter (2009), Source analysis of the Memorial Day explosion, Kimchaek, North Korea, Geophys. Res. Lett., 36(21).

Ford, S. R., W. R. Walter, and D. S. Dreger (2012), Event discrimination using regional moment tensors with teleseismic-P constraints, Bulletin of the Seismological Society of America, 102(2), pp. 867-872.

Jia, Z., S. Ni, R. Chu, and Z. Zhan (2017), Joint inversion for earthquake depths using local waveforms and amplitude spectra of Rayleigh waves, Pure and Applied Geophysics, 174(1), pp. 261-277.
Jia, Z., Z. Shen, Z. Zhan, C. Li, Z. Peng, and M. Gurnis (2020a), The 2018 Fiji Mw 8.2 and 7.9 deep earthquakes: One doublet in two slabs, Earth and Planetary Science Letters, 531, 115997.
Jia, Z., X. Wang, and Z. Zhan (2020b), Multifault Models of the 2019 Ridgecrest Sequence Highlight Complementary Slip and Fault Junction Instability, Geophysical Research Letters, 47(17), e2020GL089802.
Kanamori, H. and L. Rivera (2008), Source inversion ofWphase: speeding up seismic tsunami warning, Geophysical Journal International, 175(1), pp. 222-238.
Kennett, B. L., E. Engdahl, and R. Buland (1995), Constraints on seismic velocities in the Earth from traveltimes, Geophysical Journal International, 122(1), pp. 108-124.
Kikuchi, M. and H. Kanamori (1991), Inversion of complex body waves—III, Bull. Seismol. Soc. Am., 81(6), pp. 2335-2350.
Lay, T., L. Burdick, and D. V. Helmberger (1984), Estimating the yields of the Amchitka tests by waveform intercorrelation, Geophysical Journal International, 78(1), pp. 181-207.
Lee, E. J., P. Chen, T. H. Jordan, P. B. Maechling, M. A. Denolle, and G. C. Beroza (2014), Full-3-D tomography for crustal structure in southern California based on the scattering-integral and the adjoint-wavefield methods, Journal of Geophysical Research: Solid Earth, 119(8), pp. 6421-6451.
Ni, S., D. Helmberger, and A. Pitarka (2010), Rapid source estimation from global calibrated paths, Seismological Research Letters, 81(3), pp. 498-504.
Plourde, A. P. and M. G. Bostock (2019), Relative moment tensors and deep Yakutat seismicity, Geophysical Journal International, 219(2), pp. 1447-1462.
Savage, B., C. Morency, B. M. Covellone, A. Rodgers, and J. Tromp (2014), Short-period, anelastic and anisotropic, waveform-based 3D Middle East model to improve nuclear explosion monitoring Rep., Rhode Island University Kingston, Kingston, RI.
Simmons, N. A., S. C. Myers, G. Johannesson, and E. Matzel (2012), LLNL-G3Dv3: Global P wave tomography model for improved regional and teleseismic travel time prediction, Journal of Geophysical Research: Solid Earth, 117(B10).
Tape, C., Q. Liu, A. Maggi, and J. Tromp (2009), Adjoint tomography of the southern California crust, Science, 325(5943), pp. 988-992.
Tape, W. and C. Tape (2012), A geometric setting for moment tensors, Geophysical Journal International, 190(1), pp. 476-498.
Tape, W. and C. Tape (2013), The classical model for moment tensors, Geophysical Journal International, 195(3), pp. 1701-1720.
Tape, W. and C. Tape (2015), A uniform parametrization of moment tensors, Geophysical Journal International, 202(3), pp. 2074-2081.
Tarantola, A. (2005), Inverse problem theory and methods for model parameter estimation, SIAM.
Vavryčuk, V. and S. G. Kim (2014), Nonisotropic radiation of the 2013 North Korean nuclear explosion, Geophys. Res. Lett., 41(20), pp. 7048-7056.

Voytan, D. P., T. Lay, E. J. Chaves, and J. T. Ohman (2019), Yield estimates for the six North Korean nuclear tests from teleseismic P wave modeling and intercorrelation of P and Pn recordings, Journal of Geophysical Research: Solid Earth, 124(5), pp. 4916-4939.
Wang, D. and A. R. Hutko (2018), Relative relocations of the North Korean nuclear tests from 2006 to 2017 using the Hi-Net array in Japan, Geophysical Research Letters, 45(15), pp. 7481-7487.
Wang, X. and Z. Zhan (2020), Moving from 1-D to 3-D velocity model: automated waveform-based earthquake moment tensor inversion in the Los Angeles region, Geophysical Journal International, 220(1), pp. 218-234.
Xu, H., S. Ni, W. Liu, H. Zhu, and X. Wang (2020), Focal mechanisms of the 2017 North Korean nuclear test and its early collapse event, Geophysical Journal International, 220(2), pp. 737-752.
Zhan, Z., D. Helmberger, M. Simons, H. Kanamori, W. Wu, N. Cubas, Z. Duputel, R. Chu, V. C. Tsai, and J.-P. Avouac (2012), Anomalously steep dips of earthquakes in the 2011 Tohoku-Oki source region and possible explanations, Earth Planet. Sci. Lett., 353, pp. 121-133.
Zhang, M. and L. Wen (2013), High-precision location and yield of North Korea's 2013 nuclear test, Geophysical Research Letters, 40(12), pp. 2941-2946.
Zhang, M. and L. Wen (2015), Seismological evidence for a low-yield nuclear test on 12 May 2010 in North Korea, Seismological Research Letters, 86(1), pp. 138-145.
Zhao, L. S. and D. V. Helmberger (1994), Source estimation from broad-band regional seismograms, Bulletin of the Seismological Society of America, 84(1), pp. 91-104.
Zhu, L. and Y. Ben-Zion (2013), Parametrization of general seismic potency and moment tensors for source inversion of seismic waveform data, Geophysical Journal International, 194(2), pp. 839-843.
Zhu, L. and D. V. Helmberger (1996), Advancement in source estimation techniques using broadband regional seismograms, Bulletin of the Seismological Society of America, 86(5), pp. 1634-1641.
Zhu, L. and L. A. Rivera (2002), A note on the dynamic and static displacements from a point source in multilayered media, Geophys. J. Int., 148(3), pp. 619-627.
Zhu, L. and X. Zhou (2016), Seismic moment tensor inversion using 3D velocity model and its application to the 2013 Lushan earthquake sequence, Physics and Chemistry of the Earth, Parts A/B/C, 95, pp. 10-18.

List of Symbols, Abbreviations, and Acronyms

AFRL	Air Force Research Laboratory
AFSPC	Air Force Space Command
AFWA	Air Force Weather Agency
CLVD	Compensated Linear Vector Dipole
DC	Double Couple component of moment tensor
DiffMT	Differential Moment Tensor
gCAP	Generalized Cut-And-Paste
ISO	Isotropic component of moment tensor
PDF	Probability Density Function

DISTRIBUTION LIST

DTIC/OCP
8725 John J. Kingman Rd, Suite 0944
Ft. Belvoir, VA 22060-6218 1 cy

AFRL/RVIL
Kirtland AFB, NM 87117-5776 1 cy

Official Record Copy
AFRL/RVB/Dr. Raymond J. Willemann 1 cy